High-Pass Filtering for Thermal Data Sharpening: 2D Matrix-Based Approach for Enhanced Spatial Detail in Raster Data

Muhammad Yusuf Caesar[1*], Laila Syawalina[2]

[1]Department of Urban and Regional Planning, Universitas Bangka Belitung, Bangka Belitung 33172, Indonesia
[2]SMA Negeri 2 Tanjung Pandan, Bangka Belitung 33413, Indonesia
*Corresponding Author: muhammad.yusuf.caesar05@gmail.com
Received: 20 September 2026
Accepted: 15 Oktober 2026

Abstracts

Thermal remote sensing data generally have coarser spatial resolution than panchromatic imagery, limiting the representation of fine-scale spatial variations. This study develops a parameterized High-Pass Filtering (HPF) approach to enhance the spatial detail of Landsat 9 Band 10 thermal data from a 30 m grid to a target 15 m grid using panchromatic information from Band 8. The method applies Gaussian filtering to extract high-frequency spatial detail, followed by normalization and controlled detail injection using three α values (0.25, 0.50, and 1.00) and three σ values (1, 2, and 3), resulting in nine experimental combinations. The sharpened thermal rasters were evaluated using descriptive statistics, RMSE, MAE, Bias, R^2, Pearson correlation, and B10–PAN spatial correlation. The results show that increasing α produces more spatially focused thermal patterns and strengthens the relationship with PAN, with B10–PAN correlation increasing from approximately 0.336–0.338 before sharpening to 0.6680 at the highest tested combination. However, stronger detail injection also increases thermal variability and deviation from the original thermal values, while the mean remains relatively stable at approximately 23.05°C. Increasing σ primarily affects the filtering characteristics and valid-data coverage, with the number of valid pixels decreasing across the tested σ levels. Overall, the parameterized HPF framework provides a simple approach for investigating thermal spatial-detail enhancement while demonstrating a clear trade-off between spatial association with PAN and consistency with the original thermal data.

Keywords: High pass filter, thermal, landsat

Introduction

The spatial resolution of satellite-derived thermal information is generally coarser than that of optical and panchromatic observations, limiting the representation of fine-scale spatial variations. This limitation is particularly relevant when thermal information is used to characterize heterogeneous surfaces, where individual thermal pixels may contain multiple surface components [1], [2], [3]. Spatial sharpening and downscaling have therefore been widely investigated to enhance the spatial representation of thermal information while maintaining consistency with the original thermal data [1], [4]. For Landsat 8/9, the OLI sensor provides a 15 m panchromatic band that can be utilized as a source of higher-resolution spatial information for thermal-data enhancement [2], [5].

Pan sharpening and related spatial-enhancement approaches commonly integrate spatial information from higher-resolution imagery into lower-resolution data. Within multiresolution analysis (MRA), spatial details can be extracted from the higher-resolution image using spatial filtering and subsequently injected into the lower-resolution image [4], [5], [6]. High-pass filtering (HPF) is one of the MRA-

based approaches in which high-frequency spatial information is extracted from the panchromatic image and incorporated into the target image [4], [7]. Similar spatial-detail extraction and injection principles have also been investigated using different filtering strategies, demonstrating the importance of spatial-detail representation in image fusion [7], [8].

The characteristics of the filtering and detail-injection process can influence the balance between spatial enhancement and preservation of the original thermal information. Previous studies have shown that increasing spatial detail does not necessarily result in improved radiometric or spectral consistency, making quantitative evaluation an important component of image-sharpening studies [4], [9]. In a Gaussian-based HPF framework, the standard deviation (σ) determines the scale of the smoothing operation and consequently affects the characteristics of the extracted high-frequency detail, whereas the injection coefficient (α) determines the magnitude of the spatial detail incorporated into the target raster. The effects of filtering parameters and spatial-detail extraction have been examined in previous image-fusion studies, where different parameter settings produced variations in spatial and spectral fidelity [7], [9]. Therefore, both spatial enhancement and preservation of the original thermal information need to be considered when evaluating a sharpening approach [1].

This study develops a parameterized HPF-based approach for enhancing the spatial detail of a Landsat 9 thermal raster represented on a 30 m grid to a target 15 m grid using the panchromatic band as the source of high-frequency spatial information. The approach applies Gaussian filtering, high-frequency detail extraction, detail normalization, and controlled detail injection. Three α values (0.25, 0.50, and 1.00) and three σ values (1, 2, and 3) are evaluated, resulting in nine experimental combinations. The resulting thermal rasters are assessed using descriptive statistics, difference-based error measures, reconstruction consistency, coefficient of determination (R^2), Pearson correlation, and the spatial correlation between thermal and panchromatic data [1], [5]. This evaluation follows the general principle used in thermal sharpening and image-fusion studies, in which both preservation of the source information and enhancement of spatial characteristics are considered [6].

Material and Methods

The methodology was designed to evaluate a parameterized High-Pass Filtering (HPF) approach for enhancing the spatial detail of Landsat 9 Band 10 (B10) thermal data represented on a 30 m pixel grid toward a target 15 m pixel grid. Landsat 9 Band 10 (B10), distributed on a 30 m pixel grid, was used as the thermal input, while Band 8 (PAN) provided the 15 m target pixel grid. Spatial sharpening of thermal information commonly utilizes higher-resolution optical or panchromatic data to introduce additional spatial detail into lower-resolution thermal data [1], [10]. Quantitative evaluation is also important for assessing the consistency of the sharpened results with the original thermal information [4].

In this study, the workflow consists of thermal and panchromatic data preprocessing, spatial alignment and resampling, Gaussian filtering, high-frequency detail extraction, detail normalization, and controlled detail injection. The B10 thermal raster is first aligned to the 15 m panchromatic grid using bilinear resampling, after which high-frequency spatial information derived from the panchromatic data is incorporated into the resampled thermal raster. This follows the general principle of extracting spatial detail from a higher-resolution image and injecting it into a lower-resolution image [4], [7]. Two parameters, the injection coefficient (α) and Gaussian standard deviation (σ), are systematically varied to produce nine experimental combinations. The resulting sharpened thermal rasters are subsequently evaluated based on the preservation of the original thermal information and their spatial relationship with the panchromatic data.

Table 1. Methods used in this research

Equation	Description	Number
$PAN_{low} = G_{\sigma}(PAN)$	PANlow = Gaussian low-pass filtered panchromatic data Gσ = Gaussian filtering operation σ = Gaussian standard deviation.	(1)
$PAN_{high} = PAN - PAN_{low}$	PANhigh = high-frequency spatial detail extracted from the panchromatic data PAN = original panchromatic data PANlow = Gaussian low-pass filtered data.	(2)
$PAN_{detail} = \left[\frac{PAN_{high} - \text{mean}(PAN_{high})}{\text{std}(PAN_{high})}\right] \times \text{std}(B10)$	PANdetail = normalized high-frequency detail mean(PAN_high) = mean of high-frequency detail std(PAN_high) = standard deviation of high-frequency detail std(B10) = standard deviation of the thermal raster	(3)
$B10_{sharp} = B10_{resampled} + \alpha(PAN_{detail})$	B10sharp = sharpened thermal raster B10resampled = thermal raster resampled to the target PAN grid using bilinear PAN_detail = normalized spatial detail α = injection coefficient controlling the magnitude of injected spatial detail.	(4)
$\alpha = \{0.25, 0.50, 1.00\}$	The three injection coefficient values used in the experiment.	(5)
$\sigma = \{1, 2, 3\}$	The three Gaussian standard deviation values used in the experiment.	(6)
$RMSE = \sqrt{\left[\frac{1}{n}\sum\left(B10_i - B10_{rec,i}\right)^2\right]}$	RMSE = root mean square error B10i = original thermal value B10rec,i = reconstructed thermal value n = number of valid pixels.	(7)
$MAE = \frac{1}{n}\sum\left\|B10_i - B10_{rec,i}\right\|$	MAE = mean absolute error between the original and reconstructed thermal raster.	(8)
$Bias = \frac{1}{n}\sum\left(B10_{rec,i} - B10_i\right)$	Bias = mean difference between reconstructed and original thermal values.	(9)
$R^2 = 1 - \frac{\sum_{i=1}^{n}\left(B10_i - B10_{rec,i}\right)^2}{\sum_{i=1}^{n}\left(B10_i - \overline{B10}\right)^2}$	R^2 = coefficient of determination calculated from the residual sum of squares between the original and reconstructed thermal values. (B10 mean) = mean of the original thermal values. Accordingly, R^2 is	(10)

Equation	Description	Number
	not assumed to be equivalent to the squared Pearson correlation coefficient (r^2)	
$r_{Pearson} = \frac{\sum\left[\left(B10_i - \text{mean}(B10)\right)\left(B10_{rec,i} - \text{mean}(B10_{rec})\right)\right]}{\sqrt{\sum\left(B10_i - \text{mean}(B10)\right)^2 \times \sum\left(B10_{rec,i} - \text{mean}(B10_{rec})\right)^2}}$	Pearson correlation coefficient (r) = linear correlation between the original and reconstructed thermal raster. Values closer to ±1 indicate stronger linear association, whereas values closer to 0 indicate weaker linear association.	(11)
$r(B10, PAN) = \frac{\sum\left[\left(B10_i - \text{mean}(B10)\right)\left(PAN_i - \text{mean}(PAN)\right)\right]}{\sqrt{\sum\left(B10_i - \text{mean}(B10)\right)^2 \times \sum\left(PAN_i - \text{mean}(PAN)\right)^2}}$	B10–PAN Pearson correlation measures the linear relationship between thermal values and corresponding PAN values at the same spatial locations. The correlation is calculated for both the original B10 and sharpened B10 to quantify the change in their spatial association with the PAN image	(12)

Landsat 9 Band 10 (B10), distributed on a 30 m pixel grid, was used as the thermal input, while Band 8 (PAN) is used as the source of higher spatial detail at the target 15 m grid. The B10 raster is reprojected and resampled to the PAN grid using bilinear interpolation, producing a thermal raster aligned with the target spatial grid. The use of the 15 m panchromatic band as a source of spatial information for thermal sharpening is consistent with previous Landsat 8/9 thermal sharpening studies [1], [5] . Both datasets are then processed as two-dimensional raster matrices for subsequent filtering and sharpening operations.

The Gaussian low-pass filter is applied to the PAN raster to produce a smoothed version of the image. The Gaussian standard deviation (σ) controls the spatial scale of the smoothing operation. The difference between the original PAN and its smoothed version is then used to extract high-frequency spatial information. This subtraction-based extraction of spatial detail follows the general principle of multiresolution and filtering-based image fusion, in which high-frequency information is separated from the higher-resolution image and subsequently incorporated into the lower-resolution image [4], [7] . The resulting detail represents local spatial variations and fine-scale features that can be incorporated into the thermal raster. The extracted spatial detail is then normalized using the mean and standard deviation of the PAN

detail and the standard deviation of B10. The normalized detail is added to the resampled B10 using the injection coefficient (α), producing the sharpened thermal raster on the target 15 m grid.

This experiment uses three values of α (0.25, 0.50, and 1.00) and three values of σ (1, 2, and 3), resulting in nine HPF parameter combinations. The injection coefficient (α) was defined as an experimental control parameter representing the strength of panchromatic spatial-detail injection. Three levels (α = 0.25, 0.50, and 1.00) were selected to represent weak, moderate, and strong detail injection, respectively, enabling a controlled sensitivity analysis of the effect of injection strength on thermal-data preservation and spatial enhancement, These values were defined as experimental levels rather than as universally optimal coefficients.

The coefficient of determination (R^2) was calculated from the residual sum of squares between the original and reconstructed thermal data. Pearson correlation (r) was calculated separately to quantify their linear association.

Therefore, R^2 in this study is not interpreted as the squared Pearson correlation coefficient (r^2).

These combinations are used to examine how the strength of detail injection and the spatial scale of Gaussian filtering affect the resulting 15 m thermal raster. The sharpened thermal rasters are reconstructed to the original B10 grid using bilinear resampling before quantitative validation. This step allows the sharpened results to be compared directly with the original 30 m B10 raster using the same spatial grid. Quantitative evaluation is used to assess both the consistency of the sharpened thermal information and changes in its spatial characteristics [1], [10] . RMSE and MAE are used to measure the magnitude of differences, while Bias measures systematic differences between the reconstructed and original thermal data, R^2 measures the agreement between the reconstructed and reference thermal values based on the residual sum of squares. Pearson correlation is used to assess the linear consistency between the original and reconstructed thermal data. The spatial relationship with the PAN raster is also evaluated by comparing B10–PAN correlations before and after sharpening.

After acquiring the results, the percentage contributions were calculated using a descriptive factorial sum-of-squares decomposition of the nine α–σ experimental combinations. The observed variation in each response metric was partitioned into contributions from α, σ, and their α × σ interaction, with each component expressed as a percentage of the total sum of squares.

Results and Discussion

The results of the nine HPF experimental combinations were evaluated to examine the effects of the injection coefficient (α) and Gaussian standard deviation (σ) on the resulting thermal raster. The analysis focused on changes in the overall thermal distribution, consistency with the original B10 data, and spatial association with the panchromatic image. Descriptive statistics were first used to examine changes in thermal values and valid-data coverage, followed by quantitative evaluation using RMSE, MAE, Bias, R^2, Pearson correlation, and B10–PAN correlation. A descriptive factorial decomposition was subsequently applied to assess the relative contributions of α, σ, and their interaction to the observed variation in the response metrics.

Table 2. Descriptive statistics of the original and sharpened thermal rasters

Methods	α	σ	Valid Pixel(N)	Min (°C)	Max (°C)	Mean (°C)	Std. Dev. (°C)
Original B10	–	–	18,803,698	10.97	30.98	23.0470	1.1474
HPF	0.25	1	18,428,867	13.21	30.26	23.0519	1.1922
HPF	0.25	2	18,139,557	13.22	30.66	23.0524	1.2008
HPF	0.25	3	17,882,083	13.21	30.50	23.0526	1.2078
HPF	0.50	1	18,428,867	13.42	35.63	23.0519	1.2973
HPF	0.50	2	18,139,557	13.44	35.30	23.0524	1.3118
HPF	0.50	3	17,882,083	13.41	34.97	23.0526	1.3241
HPF	1.00	1	18,428,867	6.95	48.51	23.0519	1.6432
HPF	1.00	2	18,139,557	8.58	44.57	23.0524	1.6653
HPF	1.00	3	17,882,083	12.59	44.23	23.0526	1.6841

Table 2 presents the descriptive statistics of the original B10 raster and the nine HPF experiments in terms of overall thermal level, thermal-value variability, extreme-value range, and valid-data coverage. The mean is used to examine changes in the overall thermal level,

the standard deviation represents changes in thermal-value variability, the minimum and maximum values describe the resulting thermal range, and the number of valid pixels indicates valid-data coverage. The original B10 raster contains 18,803,698 valid pixels, with values ranging from 10.97 to 30.98 °C, a mean of 23.0470 °C, and a standard deviation of 1.1474 °C. Across all HPF combinations, the mean remains highly consistent, ranging from 23.0519 to 23.0526 °C. This indicates that the HPF procedure preserves the overall thermal level of the input raster despite the injection of spatial detail.

At α = 0.25, the standard deviation increases only slightly from 1.1922 to 1.2078 °C as σ increases from 1 to 3, while the minimum and maximum values remain relatively close to the original thermal range. At α = 0.50, the mean remains similarly stable, but the standard deviation increases to 1.2973–1.3241 °C and the maximum values increase to 34.97–35.63 °C. The largest changes occur at α = 1.00, for which the standard deviation reaches 1.6432–1.6841 °C, while the thermal range expands substantially, with minimum values of 6.95–12.59 °C and maximum values of 44.23–48.51 °C. These results indicate that increasing α primarily affects the magnitude of local thermal-value variation rather than the overall mean. In other words, stronger spatial-detail injection increases the dispersion and extreme values of the sharpened raster while leaving its mean relatively stable.

This behavior is consistent with the general characteristics of spatial-detail injection reported in previous image-fusion studies. [7] demonstrated that the extraction and transfer of high-frequency information from PAN imagery can substantially influence the spatial characteristics of the fused image, and their parameter analysis showed that filter settings affect fusion performance. Similarly, [5] found that HPF and other multiresolution-analysis methods can enhance spatial reconstruction in thermal image pan sharpening, although the resulting products still exhibit differences in radiometric quality.

Increasing variation observed in the present study is also relevant to the thermal-consistency issue reported by [11]. Their Landsat 8/9 thermal sharpening experiments showed that increasing spatial enhancement involves a balance between spatial detail and thermal consistency; their comparison found that conventional PAN-based sharpening could maintain relatively high radiometric accuracy but was weaker in spatial enhancement, whereas approaches producing stronger spatial detail could experience greater losses in thermal consistency. Therefore, the widening thermal range observed at α = 0.50 and particularly at α = 1.00 can be interpreted as evidence that stronger detail injection introduces greater local variation into the thermal raster. This does not necessarily indicate improved thermal accuracy, but rather a stronger modification of the original thermal-value distribution.

The number of valid pixels decreases as σ increases, from 18,428,867 at σ = 1 to 18,139,557 at σ = 2 and 17,882,083 at σ = 3. The same valid-pixel counts are observed across the three α values for each σ level, indicating that the variation in valid-data coverage is associated with the σ configuration rather than the injection coefficient. In contrast to α, which primarily changes the magnitude of the injected spatial detail, σ affects the filtering configuration and is associated with changes in valid-data coverage. Previous thermal pan sharpening research has likewise emphasized that filtering and parameter selection can influence the spatial and radiometric characteristics of the resulting image [4], [7] .

Table 3. Thermal preservation and spatial correlation results

α	σ	RMSE (°C)	MAE (°C)	Bias (°C)	R^2	Pearson r	B10–PAN r (Original)	B10–PAN r (Sharpened)
0.25	1	0.2870	0.1492	0.00003	0.9378	0.9706	0.3376	0.4427
0.25	2	0.2870	0.1546	0.00000	0.9380	0.9711	0.3366	0.4632

0.25	3	0.2870	0.1579	−0.00001	0.9380	0.9715	0.3356	0.4731
0.50	1	0.5740	0.2983	0.00006	0.7514	0.8969	0.3376	0.5142
0.50	2	0.5740	0.3092	0.00001	0.7519	0.8994	0.3366	0.5523
0.50	3	0.5740	0.3158	−0.00001	0.7521	0.9017	0.3356	0.5709
1.00	1	1.1479	0.5966	0.00013	0.0055	0.7157	0.3376	0.5755
1.00	2	1.1480	0.6185	0.00001	0.0074	0.7252	0.3366	0.6373
1.00	3	1.1480	0.6315	−0.00002	0.0085	0.7333	0.3356	0.6680

* Although the original B10 raster remains unchanged, its B10–PAN correlation varies slightly across σ levels because the number of valid pixels used in the calculation decreases as σ increases.

The table above presents the quantitative evaluation of the nine HPF experiments using error, consistency, and spatial-correlation metrics. Before calculating the validation metrics, each sharpened thermal raster was reconstructed to the original B10 grid using bilinear resampling, allowing direct comparison with the original thermal raster. RMSE, MAE, and Bias represent the magnitude and systematic differences, while R^2 and Pearson correlation indicate the consistency between the reconstructed and original thermal data. The B10–PAN correlation is used separately to examine changes in the spatial relationship with the panchromatic data. This separation between thermal consistency and spatial consistency follows the evaluation framework commonly applied in thermal image fusion studies [11] .

RMSE, MAE, Bias, R^2, and Pearson r evaluate the consistency between the original and reconstructed thermal data. B10–PAN correlation indicates the spatial association between the thermal raster and the panchromatic image and is interpreted as a spatial enhancement indicator rather than a measure of thermal accuracy. The distinction between R^2 and Pearson correlation (r) was particularly evident at higher injection strength. For example, at α = 1.00 and σ = 3, the reconstructed thermal data produced an R^2 of 0.0085, whereas Pearson correlation reached 0.7333. This indicates that the reconstructed data maintained a relatively strong linear association with the original thermal data, while still exhibiting substantial deviations in absolute values.

Because the PAN image is the source of the injected spatial detail, an increase in B10–PAN correlation is expected when the HPF process successfully transfers PAN-derived spatial variation into the thermal raster. Therefore, B10–PAN correlation is used in this study only as a supporting indicator of increased spatial association with the high-resolution PAN image, rather than as an independent measure of thermal accuracy. Thermal consistency is evaluated separately using RMSE, MAE, Bias, R^2, and Pearson correlation, while spatial characteristics are further examined through the spatial patterns of the sharpened rasters.

For α = 0.25, RMSE remains approximately 0.2870 °C, while R^2 remains high at 0.9378–0.9380 and Pearson correlation at 0.9706–0.9715. At the same time, B10–PAN correlation increases from approximately 0.336–0.338 to 0.4427–0.4731 after sharpening. This indicates that relatively weak detail injection can increase the spatial relationship with PAN while maintaining high consistency with the original thermal raster. This pattern is consistent with previous thermal pan sharpening studies showing that multiresolution-based approaches can improve spatial reconstruction while retaining relatively strong radiometric consistency [4], [12] . In their thermal-image experiment, HPF also produced relatively strong spatial reconstruction, although differences in dataset and evaluation metrics prevent direct comparison of the numerical values.

When using α = 0.50, RMSE increases to approximately 0.5740 °C, while R^2 decreases to 0.7514–0.7521 and Pearson correlation to 0.8969–0.9017. Conversely, B10–PAN correlation increases to 0.5142–0.5709. The same pattern becomes stronger at α = 1.00, where RMSE reaches approximately 1.1480 °C

and R^2 decreases to only 0.0055–0.0085, while B10–PAN correlation reaches 0.5755–0.6680. These results demonstrate a clear trade-off: stronger injection produces a stronger spatial relationship with PAN but greater deviation from the original thermal raster. A similar trade-off was reported by [11], who found that thermal sharpening methods may differ substantially in the balance between spatial enhancement and thermal consistency.

Across σ = 1–3, the changes were considerably smaller than those produced by α. For example, at α = 0.50, B10–PAN correlation increased from 0.5142 to 0.5709, whereas R^2 changed only from 0.7514 to 0.7521. This indicates that α has a stronger influence on the magnitude of the thermal–spatial trade-off in this experiment, while σ produces more gradual changes. This is generally consistent with filtering-based fusion research showing that filter parameters influence the resulting spatial-detail characteristics [7]. To further quantify the relative influence of the two experimental parameters, a descriptive factorial effect decomposition was performed across the nine α–σ combinations. The analysis separated the observed variation in each response metric into contributions from α, σ, and their α × σ interaction. Because each parameter combination represents a single experimental result and the raster observations are spatially dependent, this decomposition was used as a descriptive sensitivity analysis rather than an inferential statistical test.

Table 4. Descriptive factorial effect decomposition of α, σ, and their interaction.

Metric	α contribution (%)	σ contribution (%)	α × σ interaction (%)
RMSE	100.000	0.000	0.000
MAE	99.754	0.191	0.055
Bias	7.931	71.609	20.460
R^2	99.9997	0.0002	0.0002
Pearson r	99.828	0.093	0.079
B10–PAN r	86.415	11.509	2.077
Std. Dev. (°C)	99.628	0.327	0.046

*The percentage decomposition of Bias should be interpreted cautiously because the absolute variation in Bias across the nine experiments is very small.

This decomposition showed that α was the dominant contributor for most thermal-consistency metrics. α accounted for 100.000% of the observed variation in RMSE, 99.754% in MAE, 99.9997% in R^2, 99.828% in Pearson r, and 99.628% in thermal standard deviation. For the B10–PAN spatial correlation, α remained the dominant contributor (86.415%), while σ contributed 11.509% and the α × σ interaction contributed 2.077%. These results quantitatively support the interpretation that α primarily controls the magnitude of injected spatial detail, whereas σ has a comparatively smaller influence on thermal-consistency metrics but a more noticeable influence on the spatial relationship with PAN.

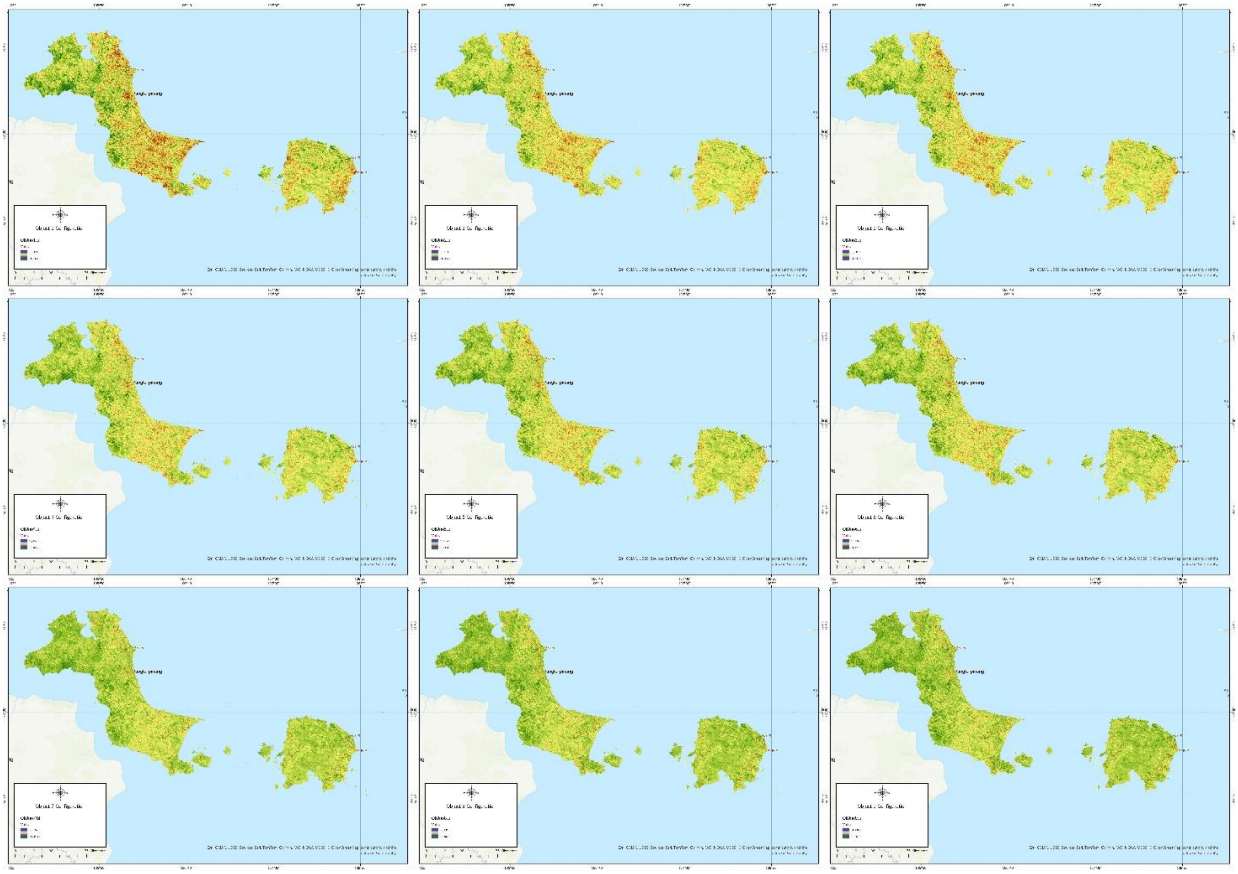


Figure 1. Spatial comparison of the nine HPF-sharpened thermal rasters generated using different α and σ combinations

The spatial distribution of the thermal data across the Bangka Belitung Islands shows noticeable changes with variations in the HPF parameters. Increasing σ is associated with a reduction in the number of valid pixels, particularly in the spatial extent of the filtered output, resulting in more limited valid-data coverage. In contrast, increasing α produces more pronounced changes in the local thermal-value distribution and spatial contrast. The observed spatial differences therefore reflect the different roles of the two parameters in the HPF process.

Increasing α produces a more pronounced effect on the spatial appearance and local distribution of thermal values. At the lower injection coefficient alpha (α = 0.25), thermal patterns in areas such as Bangka Regency, South Bangka Regency, and East Belitung Regency appear relatively diffuse and blurry, with high-temperature areas represented by broader red regions and less distinct spatial contrasts. At the highest injection coefficient alpha, where α reaches 1.00, the thermal patterns appear more spatially detailed and concentrated. High-temperature areas that previously appeared broadly distributed become more localized and spatially focused, producing more pronounced spatial contrasts across the study area.

This increase in spatial detail is accompanied by a wider range of thermal values. At α = 0.25, the maximum values range from 30.26 to 30.66°C, whereas at α = 1.00, the maximum values increase to 44.23–48.51°C. The minimum values also extend farther from the original thermal range at higher α values. Despite these changes, the mean thermal value remains highly stable at approximately 23.05°C. This indicates that increasing α does not substantially alter the overall thermal level of the study area, but instead increases local thermal variability and strengthens spatial contrasts within the raster.

Overall, the spatial results indicate that σ primarily affects the spatial characteristics and valid-data coverage of the filtering process, whereas α controls the magnitude of spatial

detail injected into the thermal raster. Higher α values produce more focused and spatially distinct thermal patterns, particularly in Bangka Regency, South Bangka Regency, and East Belitung Regency, but also generate increasingly extreme thermal values and increase range. Thus, greater spatial detail is accompanied by greater deviation from the original thermal-value range, even though the overall mean remains largely preserved.

Conclusion

This study demonstrates that a parameterized High-Pass Filtering approach can enhance the spatial detail of Landsat 9 Band 10 thermal data represented on a target 15 m grid through controlled injection of panchromatic spatial detail. Across the nine experimental combinations, increasing the injection coefficient (α) produced stronger spatial association with the PAN image and more pronounced spatial patterns, but also increased thermal-value variability and deviation from the original thermal data. In contrast, the Gaussian standard deviation (σ) primarily influenced the filtering characteristics and valid-data coverage, with a comparatively smaller effect on thermal-consistency metrics. The descriptive factorial analysis further showed that α was the dominant contributor to the observed variation in RMSE, MAE, R^2, Pearson correlation, and thermal standard deviation, and also remained the dominant contributor to B10–PAN correlation. Overall, the results demonstrate a clear trade-off between spatial-detail enhancement and consistency with the original thermal information, with α primarily controlling the magnitude of this trade-off. The proposed HPF framework therefore provides a simple parameterized approach for investigating the spatial enhancement of thermal raster data without requiring machine-learning-based methods.

References

[1] M. K. Firozjaei, M. Kiavarz, and S. K. Alavipanah, "Satellite-derived land surface temperature spatial sharpening: A comprehensive review on current status and perspectives," Eur. J. Remote Sens., vol. 55, no. 1, pp. 644–664, 2022, doi: 10.1080/22797254.2022.2144764.

[2] M. Z. Dahiru, M. Hashim, and N. Hassan, "Sharpening of thermal satellite imagery from klang industrial area in peninsular malaysia using the tsharp approach," in International Archives of the Photogrammetry, Remote Sensing and Spatial Information Sciences - ISPRS Archives, International Society for Photogrammetry and Remote Sensing, Jan. 2022, pp. 87–102. doi: 10.5194/isprs-archives-XLVI-4-W3-2021-87-2022.

[3] D. Roy et al., "Assessing the accuracy of multi-model approaches for downscaling land surface temperature across diverse agroclimatic zones," Sci. Rep., vol. 15, no. 1, Dec. 2025, doi: 10.1038/s41598-025-92135-0.

[4] J. Raimundo, S. L. C. Medina, J. F. Prieto, and J. A. de Mata, "Super resolution infrared thermal imaging using pansharpening algorithms: Quantitative assessment and application to uav thermal imaging," Sensors (Switzerland), vol. 21, no. 4, pp. 1–18, Feb. 2021, doi: 10.3390/s21041265.

[5] J. Raimundo, S. Lopez-Cuervo Medina, and J. F. Prieto, "Resolution enhancement of infrared thermal imaging by pansharpening algorithms," in International Archives of the Photogrammetry, Remote Sensing and Spatial Information Sciences - ISPRS Archives, International Society for Photogrammetry and Remote Sensing, Sep. 2021, pp. 593–599. doi: 10.5194/isprs-archives-XLVI-M-1-2021-593-2021.

[6] E. Alcaras and C. Parente, "The Effectiveness of Pan-Sharpening Algorithms on Different Land Cover Types in GeoEye-1 Satellite Images," J. Imaging, vol. 9, no. 5, May 2023, doi: 10.3390/jimaging9050093.

[7] A. A. L. Smadi, S. Yang, A. Mehmood, A. Abugabah, M. Wang, and M. Bashir, "Smart pansharpening approach using kernel-based image filtering," IET Image Process., vol. 15, no. 11, pp. 2629–2642, Sep. 2021, doi: 10.1049/ipr2.12251.

[8] X. Liu, P. Tang, X. Jin, and Z. Zhang, "From Regression Based on Dynamic Filter Network to Pansharpening by Pixel-Dependent Spatial-Detail Injection," Remote Sens. (Basel)., vol. 14, no. 5, Mar. 2022, doi: 10.3390/rs14051242.

[9] T. Liu et al., “A novel pansharpening method based on side window filter and new injection gain matrices,” Sci. Rep., vol. 15, no. 1, Dec. 2025, doi: 10.1038/s41598-025-08929-9.
[10] K. Zhang et al., “Panchromatic and multispectral image fusion for remote sensing and earth observation: Concepts, taxonomy, literature review, evaluation methodologies and challenges ahead,” Information Fusion, vol. 93, pp. 227–242, May 2023, doi: 10.1016/j.inffus.2022.12.026.
[11] L. Alparone and A. Garzelli, “Downscaling Land Surface Temperature via Assimilation of LandSat 8/9 OLI and TIRS Data and Hypersharpening,” Remote Sens. (Basel)., vol. 16, no. 24, Dec. 2024, doi: 10.3390/rs16244694.
[12] W. Li, Y. Hu, Y. Peng, and M. He, “A Swin Transformer with Dynamic High-Pass Preservation for Remote Sensing Image Pansharpening,” Remote Sens. (Basel)., vol. 15, no. 19, Oct. 2023, doi: 10.3390/rs15194816.